18TH WORLD CONFERENCE ON EARTHQUAKE ENGINEERING
WCEE2024
MILAN

MILAN, ITALY
30TH JUNE - 5TH JULY 2024
www.wcee2024.it

CORROSION-INDUCED FAILURE MODE ALTERATIONS AND IMPLICATIONS ON SEISMIC FRAGILITY OF RC FRAMES

S. Shekhar[1], F. Freddi[2], J. Ghosh[3], D. Lad[2]

& R. Chelapramkandy[3]

[1] Indian Institute of Technology Mandi, Mandi, India, shivang@iitmandi.ac.in

[2] University College London, London, United Kingdom

[3] Indian Institute of Technology Bombay, Mumbai, India

Abstract: *This study evaluates the influence of corrosion deterioration on the change in failure modes and subsequent impact on the seismic fragility of low-ductility reinforced concrete (RC) building frames. A three-story, three-bay, low-ductility RC frame is selected, and a detailed numerical model is developed by accounting for the nonlinear behavior of different components and time-dependent corrosion deterioration. The developed numerical model can capture the non-ductile failure modes of low-ductility RC frames designed without consideration of modern seismic design and detailing principles. Non-linear time-history analysis results reveal a change in the failure mode of RC columns within the frame from flexure to flexure-shear and an increase in the column peak drift due to corrosion. Time-varying probabilistic seismic demand models and damage state thresholds are used to develop seismic fragility curves. Results indicate that at the end of the design service life (50 years), corrosion deterioration significantly increases the seismic fragility by up to 38% for the Complete damage state.*

1 Introduction

The structural performance of reinforced concrete (RC) buildings is significantly affected by durability concerns arising from exposure to harsh environmental conditions. Buildings located in extreme environmental conditions experience aging and deterioration of RC components due to corrosion leading to a substantial reduction in the embedded steel rebars cross-sectional area, along with other secondary effects. Corrosion can significantly lower the lateral load-carrying capacity and ductility of RC buildings. Previous research has shown that 70-90% of the degradation in RC buildings results from the corrosion of RC components (Angst, 2018). Additionally, the global cost of corrosion deterioration is estimated to be approximately 2.5 trillion USD, equivalent to 3.4% of the worldwide Gross Domestic Product (GDP) (Koch *et al.*, 2016). Furthermore, in addition to continuous exposure to environmental hazards, when located in moderate to high seismic regions, RC buildings also experience intermittent earthquake threats throughout their service life. Old and non-ductile RC buildings have suffered substantial damage in past earthquakes worldwide, leading to extensive economic and human losses. For instance, the 1976 Tangshan earthquake, resulted in 255,000 casualties and 10 billion USD loss, while the 2011 Tohoku earthquake resulted in 30,000 casualties and a 235 billion USD loss (Davis *et al*., 2012; Wu *et al*., 2014). The magnitude of these losses may be expected to be higher when buildings are designed with non-seismic design standards and undergoing corrosion deterioration. Acknowledging this critical aspect, researchers have recently focused on the seismic performance evaluation of deteriorating RC buildings using time-dependent seismic fragility curves.

Recognizing the need for studying the influence of corrosion on the lifetime seismic performance of existing RC buildings, recently few numerical studies have been conducted on RC moment resisting frames. Pitilakis *et al*. (2014) conducted a detailed study on low-, mid-, and high-rise moment-resisting frames by considering probabilistic modeling of corrosion deterioration. The results reveal that the time-dependent corrosion

deterioration significantly influences the seismic performance of the RC frames. Couto *et al*. (2020) assessed the effects of varying corrosion rates on seismic fragility of aging RC building frames constructed in Portugal from 1960 to 1980. Results showed up to a 20% increase in failure probability due to corrosion, with concrete strength degradation notably influencing the seismic capacity as compared to the reduction in rebar area. Di Sarno & Pugliese, (2020a) analyzed the seismic response of an RC building under different exposure and degradation conditions, including corrosion-induced reductions in rebar area and material properties. Results revealed increased roof and inter-story drift ratios along with significant reduction in base shear capacity due to corrosion. This leads to early collapse of buildings especially at high corrosion levels. Dizaj *et al*. (2018) explored the influence of non-uniform corrosion on the seismic fragility of code-conforming and non-conforming RC frames, concluding that spatial variability had negligible effects on global seismic response. Other researchers also noted corrosion's impact on RC frames subjected to multiple seismic events (Di Sarno & Pugliese, 2020b). These studies advance the understanding of aging building structures but do not explore corrosion's effects on specific failure modes within RC elements (*e.g.,* shear failure, flexure-shear failure, and flexure failure), a critical aspect in aged non-seismically designed (low-ductile) RC buildings suffering from corrosion deterioration. Past experimental studies have highlighted the possible change in failure modes of RC columns from flexure to shear due to corrosion deterioration (Vu & Li, 2018), thereby highlighting the need to incorporate these effects into the numerical model for seismic vulnerability assessment.

Addressing this issue, the present study aims to evaluate the influence of corrosion deterioration on the seismic vulnerability of RC frames utilizing detailed numerical models that can capture varied failure modes of low-ductility RC frames. The paper is organized as follow: Section 2 presents the details of the case-study frame including location-specific probabilistic deterioration model to simulate the time-dependent corrosion degradation of the case-study frame. This section also provides details of the finite element (FE) model that can accurately represent the various failure modes of the deteriorated frame. Section 3 presents the influence of corrosion deterioration on the seismic response and failure modes using non-linear time-history analyses (NLTHAs). Section 4 describes the results of the NLTHAs conducted by using a large set of ground motions to capture record-to-record variability and capacity estimates of different damage states (*DSs*). Time-varying seismic fragility curves are developed for the as-built and 50-year frames. Finally, Section 5 presents the key findings and direction for future works.

2 Case-study frame, corrosion deterioration and finite element (FE) modeling

This study illustrates the influence of lifetime corrosion deterioration on the change in failure modes and seismic fragility using a representative low-ductility frame assumed to be located in coastal California, US. The case-study structure, characterized by lack of seismic design considerations, is representative of construction practices employed in US prior to the implementation of contemporary seismic design codes. Beyond the concerns related to earthquake threats, corrosion-induced deterioration substantially impacts the load-carrying capability of these low-ductility structures, potentially resulting in vulnerable brittle failure modes during seismic events.

2.1 Case-study frame

Figure 1 shows the layout of the selected case-study frame adopted from Bracci *et al*. (1995). This three-story, three-bay RC frame is representative of low-rise RC buildings that were designed without seismic design considerations (low ductility). The building frame has a total height of 10.75 m with a constant inter-story height of 3.66 m, and bay width of 5.49 m. The frame is designed only for gravity loads as per ACI-318-89 (1989), with 300 × 300 mm columns and 230 × 460 mm beams on each floor. The RC members are designed with 24 MPa compressive strength and Grade 40 (yield strength of 276 MPa) longitudinal reinforcing steel. The reinforcement details for the case-study frame, as depicted in Figure 1, reveal deficiencies in the columns and beam-column joints, including insufficient transverse reinforcement, inadequate anchorage length and hooks for reinforcement, and presence of lap splices in areas prone to plastic hinge formation.

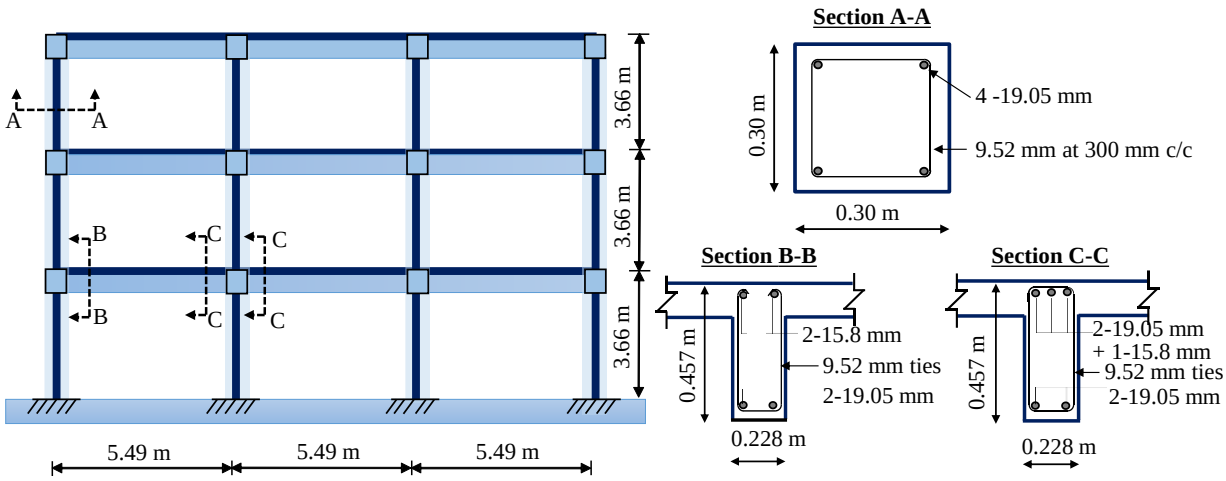

Figure 1. Case-study RC frame adapted from Bracci et al. (1995) and Aycardi et al. (1994).

2.2 Time-dependent deterioration modeling

In adverse environmental conditions, RC buildings undergo time-dependent aging and degradation, primarily in the form of corrosion and other physical and chemical deterioration. Among these, chloride ion-induced corrosion is a predominant mode of degradation for RC structures (Stewart & Rosowsky, 1998). Chlorides originate from marine environments and airborne sources, which are prevalent exposure scenarios for RC buildings in the coastal region of California (Zhang *et al.*, 2022). Therefore, this study focuses on chloride-induced corrosion as the primary time-dependent degradation mechanism for the case-study building frame, with the selected exposure scenario representing a high level of deterioration (Thoft-Christensen, 2004).

Corrosion in RC structures commence after a specific duration known as the corrosion initiation time (T_{init}). During this period, chloride ions gradually penetrate the concrete cover, causing depassivation of the reinforcing steel and initiating corrosion. This study employs the widely recognized probabilistic model introduced by Duracrete (2000) to predict the corrosion initiation time. Based on the uncertainty of deterioration parameters (such as diffusion coefficient, critical chloride concentration, surface chloride concentration, curing and test correction factors, and concrete cover depth, among others), a Monte Carlo simulation is conducted to estimate the mean corrosion initiation time for both longitudinal and transverse reinforcement of RC elements. Subsequently, a lognormal distribution is found to be a suitable representation of the statistics of corrosion initiation time. Specifically, a lognormal distribution with a mean of 10 years closely matches the simulated data for the corrosion initiation time of transverse steel reinforcement, which has an average cover depth of 38.1 mm. Similarly, the mean corrosion initiation time for longitudinal steel reinforcement is estimated to be 14 years. It's worth noting that the transverse steel reinforcement is expected to experience a shorter initiation time compared to the longitudinal reinforcement due to the reduced concrete cover (refer to Figure 1).

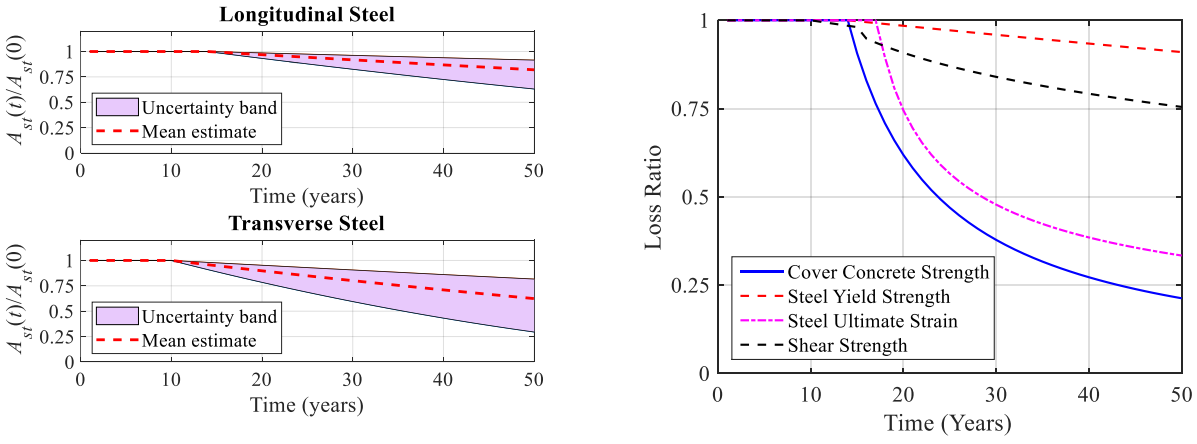

(a) (b)

Figure 2. Time-dependent variation of (a) longitudinal and transverse steel area, and (b) steel strength, ultimate strain, concrete cover strength, and shear strength of RC columns.

After the initiation phase, the corrosion propagation stage is characterized by the development of small independent pits or cracks on the steel rebar. Over time, these defects expand, leading to broader cracks and ultimately resulting in uniform corrosion. The propagation phase corrosion rate is also adopted from Duracrete (2000), with mean corrosion rate of 2.586 $\mu A/cm^2$, and coefficient of variation of 0.66. Utilizing the corrosion rate, the mean reduction in cross-section of longitudinal and transverse reinforcing steel over the design service life of 50 years is estimated and shown in Figure 2 (a). Also, shown in the figure is the lower and upper limits of the uncertainty band, representing the 5^{th} and 95^{th} percentile confidence bounds after considering uncertainties in the corrosion deterioration process. The impact of area loss in reinforcement is more visible for smaller diameter rebars (Stewart, 2004), resulting in a higher percentage of area loss observed in transverse steel, as evident in the figure. After 50 years, a reduction in area loss of 19% for longitudinal reinforcement and 38% for transverse reinforcement in columns is observed.

It is important to note that this study does not consider the complexities of non-uniform pitting corrosion in steel reinforcement. However, following the recommendations of Dizaj *et al*. (2018), the effects of non-uniform pitting corrosion, such as reductions in steel strength and ductility, are explicitly accounted for in the deteriorated frame modeling. This study employs Du *et al*. (2005) linear model to depict the decrease in steel strength due to percentage mass loss of reinforcing steel. Past experimental observations reveal that reduction of ultimate strain of steel follows a non-linear pattern (Andisheh *et al*., 2016), therefore, this study incorporates findings from Apostolopoulos and Papadakis (2008) that relates ultimate strain reduction to the percentage mass loss in reinforcing steel. Additionally, rebar corrosion leads to expansive rust products, causing micro-cracks, weakening of cover concrete, and potentially causing spalling. Cover concrete strength deterioration is estimated based on the Coronelli and Gambarova (2004) model. The transverse reinforcement corrosion deterioration leads to reduction in shear strength of RC columns and can escalate the risk of change in flexure failure modalities to flexure-shear or shear failures. The time-dependent loss of shear strength in RC columns is determined using the model introduced by Vu and Li (2018). This model considers multiple member attributes, including concrete compressive strength, aspect ratio, core and cover concrete areas, transverse steel reinforcement area and yield strength, and axial load on the column. Figure 2 (b) shows the mean reduction in the steel strength, ultimate steel strain, concrete cover strength, and shear strength, respectively. At the end of design service life, the deteriorated RC columns undergoes 10%, 67%, 79%, and 25% reduction in the above-mentioned parameters.

2.3 FE modeling incorporating corrosion deterioration

A two-dimensional FE model of the case-study frame is developed using OpenSees (McKenna *et al*., 2000). This model aims to simulate both the overall system-level behavior and the seismic response of individual components, especially those susceptible to brittle failures as observed in low-ductility RC moment resisting frames. This approach allows capturing local failure mechanisms and assess the influence of corrosion-related deterioration of building components on the global response parameters.

Figure 3 illustrates the FE model, highlighting key modeling details of structural components such as columns, beams, and joints. Columns nonlinear flexural response is captured using the *nonLinearBeamColumn* element, with concrete unconfined and confined fiber sections modeled using the *Concrete02* material model. The longitudinal steel reinforcements in the RC fiber sections are modeled using the *uniaxialMaterial Hysteretic* model, calibrated to capture pinching behavior based on the experimental results of Aycardi *et al*. (1994). Beams are modeled using *beamWithHinges* element, which comprises a central elastic element and two plastic hinge regions located at the element's ends defined using fiber sections similar to the columns. The slabs are modeled with an effective width equal to four times the width of the beams. The gravity loads are applied to beams, and masses are concentrated at beam-column intersections.

For the deteriorated RC beams and columns, the FE model incorporates the effects of chloride-induced corrosion and associated uncertainties. The steel area loss from corrosion is modeled as a uniform reduction in rebar diameter that accounts for time-dependent corrosion rate uncertainty. The FE modeling of the deteriorated frame also addresses secondary effects, such as reduced rebar strength and ductility, along with cover and core concrete strength reduction. To capture these effects in the corroded frame, the time-dependent reductions in rebar strength and ductility is estimated and the *Hysteretic* steel material parameters are updated. Furthermore, the decrease in core concrete strength due to transverse reinforcement corrosion and the loss of cover strength from expansive rust product formation is incorporated by updating *Concrete02* material parameters.

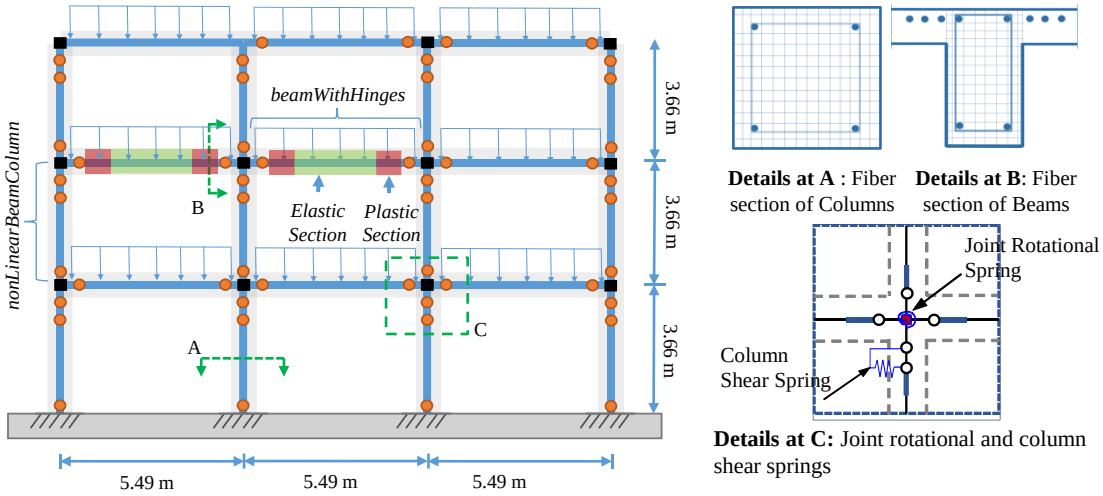

Figure 3. Numerical modeling of the case-study frame highlighting modeling details of columns and beams fiber sections, column shear springs, and joint rotational springs

While the fiber section-based RC modeling captures non-linear flexural deformation, in low-ductility frames the non-linear behavior can also arise from column shear failure and the loss of gravity load-bearing capacity (Elwood, 2004). To address this, zero-length shear springs (element *zeroLength* in OpenSees) are introduced in series with column flexure elements, as illustrated in Figure 3. These springs use the uniaxial *LimitState* material model and trigger when the column response reaches either predefined shear strength or drift limit curves (implemented as *limitCurve* Shear in OpenSees) (Freddi *et al*., 2021; Shekhar *et al*., 2020). The shear strength limit curve is based on ASCE-41, and the deformation limit curve follows an empirically derived force-deformation controlled limit curve by Elwood (2004). Both strength and drift shear limit curves depend on various parameters, including column transverse reinforcement, axial load, section dimensions, and material properties, all influenced by column corrosion. A two-node *zeroLength* rotational joint spring, and four rigid offsets are used to model the behavior of low-ductility joints of the RC frame with the *Pinching4* material model employed to address pinching behavior in joint responses (Jeon *et al*., 2015). Notably, the study presently excludes the consideration of corrosion effects on joint behavior and is left for future exploration. Further details on the validation of numerical model can be found in Freddi *et al*., (2013, 2021) and Shekhar *et al*., (2023).

3 Corrosion deterioration influence on seismic response and failure mechanism

To assess the impact of corrosion on the seismic response and failure modalities, the case-study frame in the as-built and 50-year deteriorated state is subjected to the ground motion acceleration time-histories to conduct NLTHAs. These ground motion are adopted from the SIMBAD database (Smerzini *et al*., 2014) consisting of records from 130 shallow crustal earthquake records across the globe with moment magnitudes ranging from 5 to 7.3 and epicenter distances less than 35 km. For the deterministic analysis, the parameters of the as-built and 50-year corroded frames are set at the mean values, where corrosion in 50-year frame results in 19% reduction in steel reinforcement area along with other secondary effects such as reduced concrete core and cover strength reduction, as well as reduced steel strength and ductility. Figure 4 (a) shows the comparison of seismic response of ground story Column 1 (shown in the inset) for the as-built and 50-year corroded frame using a ground motion accelerogram with *PGA* = 0.30g. For this accelerogram, column peak drift increases by about 127.2% after 50 years of corrosion exposure compared to the as-built column. It is worthwhile to note that the hysteresis loop of the 50-year corroded column intersects the drift-based shear limit curve highlighting the onset of flexure-shear failure. However, for the as-built case the hysteretic loop does not reach either force or drift shear limit curve, thereby showing flexure behavior. A similar change in failure mechanism due to corrosion is also seen in Figure 4 (b) for Column 1 considering another ground motion accelerogram of *PGA* = 0.48 g. For 1st story Column 7, similar change in failure mechanism from flexure to flexure-shear is also observed as shown in Figure 4 (c).

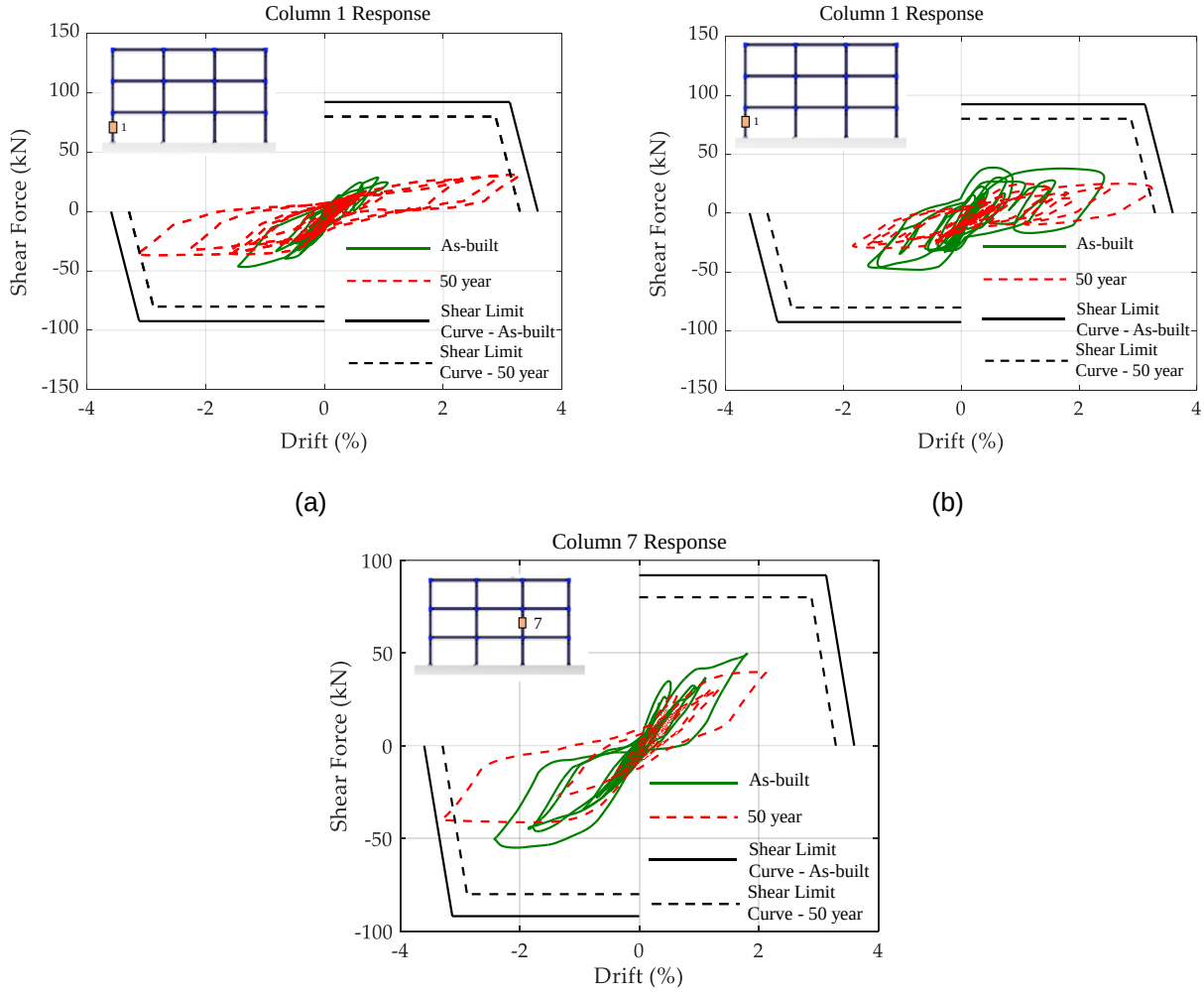

Figure 4. Comparison of seismic response of as-built and 50-year corroded frame columns.

4 Time-dependent seismic fragility analyses

The preceding section presents the time-dependent seismic response comparison of an as-built and deteriorated frames when subjected to two different ground motions. However, due to inherent randomness in the deterioration parameters along with ground motions, a full probabilistic analysis is required to determine the effect of corrosion on building frame seismic vulnerability. Typically, the extent of damage is represented by fragility curves that indicate the probability of demand greater than capacity given the intensity of ground motion. The time-dependent seismic fragility curves are developed for as-built and deteriorated frames for four distinct *DSs* – Slight, Moderate, Extensive, and Complete. These curves are derived by assessing the seismic demand and capacities of nominally similar, yet statistically different FE frame models, accounting for uncertainty related to corrosion degradation. The seismic fragility curves for as-built, and 50-year frames are constructed using the Cloud Analysis approach (Cornell *et al*., 2002), which employs probabilistic seismic demand models (PSDMs) and different *DSs* capacity limits or thresholds. The following section provides further details of the PSDMs, *DSs* thresholds, and time-dependent seismic fragility curves.

4.1 Probabilistic seismic demand and capacity models

PSDMs relates the median peak engineering demand parameter (*EDP*) of the building frame with the intensity measure (*IM*) of the ground motion and are developed by conducting NLTHAs of the building frame by using the selected set of ground motion records. For development of PSDMs, a set of 150 ground motion records are adopted from SIMBAD database with minimum and maximum PGA as 0.21g and 1.78g, respectively. Although not region-specific, the chosen ground motion records offer a wide range of earthquake ground motions characteristics for generic assessment of the seismic behavior of corroded RC frames. The 150

ground motions are paired randomly with the 150 FE models generated using Latin Hypercube sampling considering uncertaility in deterioration parameters. Following the NLTHAs, PSDMs are developed to estimate median seismic demand as function of ground motion intensity measure as (Cornell *et al*., 2002):

$$\ln\left[EDP_{med}(t)\right] = \ln[a(t)] + b(t)\ln(IM) \quad (1)$$

where, $EDP_{med}(t)$ is the median estimate of *EDP* (taken as maximum inter-story drift, IDR_{max}), $\ln[a(t)]$ and $b(t)$ are the regression coefficients at a particular year (as-built, and 50-year) along the service life, and *IM* is the intensity measure. A proper *IM* is crucial for development of accurate PSDM and fragility curves, and past researchers have suggested $S_a(T_1)$ as the optimal *IM*. However, corrosion in RC beams and columns can elongate the time period due to reduced rebar area and cover concrete strength leading to increase in the fundamental time period from 1.12 s to 1.30 s, respectively. Therefore, to enable direct comparisons of PSDMs and fragility curves for different frames, the average spectral acceleration ($S_{a,avg}$) is adopted as *IM* based on the suggestion of recent work carried out by the authors (Shekhar *et al*., 2023). The regression based PSDM [Equation (1)] also provides zero mean model fitting error *i.e.* dispersion in demand (β_D) required for fragility development. Table 1 provides the complete list of PSDMs parameters [ln (a), b, β_D] for as-built and 50-year frames. It can be observed that for 50-year frame PSDMs has higher slope (indicating higher demand) and dispersion compared to the as-built frame. The table also reports the goodness of fit measure in terms of R^2 for the developed PSDMs, with high value indicating the adequacy of the chosen intensity measure in predicting the frame IDR_{max}.

Table 1. PSDMs linear regression coefficients for as-built, and 50-year frames.

Frame	ln (a)	b	β_D	R^2
As-built	1.62	0.89	0.25	0.94
50-year	1.82	0.95	0.38	0.87

Following the development of PSDMs at different years, capacity limits or thresholds for various *DSs* are developed using non-linear static (pushover) analyses. The time-varying corrosion deterioration effects of beams and columns such as reduction in rebar area along with decrease in mechanical properties of steel and concrete impact the lateral load-resisting capacity of the frame. Therefore, this study estimates capacity limit in terms of IDR_{max} for the various *DSs* by assessing multiple failure criteria in terms of local *EDPs* such as material strains in beams and columns, and local failure mechanisms such as shear failure of columns. The Slight *DS* is associated with column yielding and is defined quantitatively by the IDR_{max} when 50% of columns at one story yield. The Moderate *DS* pertains to the crushing or spalling of concrete in columns and is quantitatively described by the IDR_{max} when the spalling strain reaches 0.004 in 50% of columns at one story. The Complete *DS* is marked by the onset of shear failure in 50% of columns at one story. For the Extensive *DS*, the IDR_{max} is calculated as the average of the IDR_{max} values corresponding to the Moderate and Complete *DSs*. A Monte Carlo approach is employed to determine probability distributions for different *DSs*, taking into account uncertainty in deterioration parameters. Pushover analyses are conducted on the RC frame samples developed using parameters obtained using MC simulations, and different *DSs* are recorded based on the failure criteria mentioned earlier. An additional lognormal standard deviation of 0.35 is also considered to account for epistemic uncertainty. Figure 5 (a) depicts the relationship between base shear and IDR_{max} plot for the RC frame in as-built, and 50-year condition for one such simulation. The figure also shows the markers corresponding to different *DSs*. It can be observed that corrosion-induced deterioration reduces the load-carrying capacity of the corroded frame, with corresponding reduction in IDR_{max} limits for different *DSs*. Figure 5 (b) depicts the lognormal fit to the IDR_{max} obtained using Monte Carlo simulations-based pushover analyses for various *DSs* of as-built and 50-year corroded frames. It can be observed that there is significant decrease in the median estimate of various *DSs* for 50-year frame compared to the as-built frame. Table 2 shows the list of median and dispersion for all *DSs* of as-built and 50-year frames. The median IDR_{max} values for the 50-year frame are 19% lower for Slight *DS*, 43% lower for Moderate *DS*, 30% lower for Extensive *DS*, and 24% lower for Complete *DS* when compared to the values of the as-built frame.

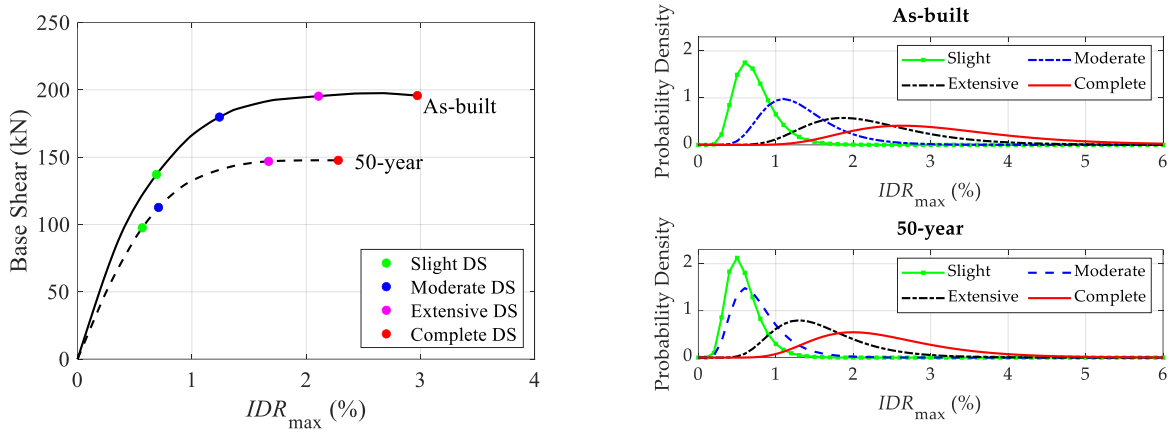

(a) (b)

Figure 5. (a) Base shear vs. IDR_{max} plot, and (b) DSs distribution for as-built and 50-year frames.

Table 2. Damage states thresholds for as-built, and 50-year frames.

Frame	Slight		Moderate		Extensive		Complete	
	Median	***Dispersion***	***Median***	***Dispersion***	***Median***	***Dispersion***	***Median***	***Dispersion***
As-built	0.690	0.350	1.240	0.350	2.110	0.350	2.970	0.350
50-year	0.555	0.360	0.714	0.410	1.482	0.362	2.252	0.348

4.2 Seismic fragility curves of as-built and corroded frames

The seismic fragility curves are developed for as-built, and 50-year frame utilizing the results of the PSDMs and the *DS* thresholds. Given the assumption that seismic demand follows lognormal distributions along with thresholds for *DSs*, the time-evolving seismic fragility curves for a specific *DS* can be expressed as:

$$Pf_{DS|IM}(t) = \Phi\left\{\frac{\ln(IM) - \ln(med(t))}{\zeta(t)}\right\} \tag{2}$$

where, $Pf_{DS|IM}(t)$ represents the seismic fragility of a *DS* at a specific point in time along the design service life, and *med(t)* and *ζ(t)* represent the median and dispersion of the fragility curves. Figure 6 (a) shows the comparison of Moderate and Complete fragility curves for the as-built, and 50-year frames. It can be observed that for both *DSs* a significant increase in the vulnerability of 50-year corroded frame is observed compared to the as-built frame. The exposure to chlorides leads to the degradation of the RC frame, resulting in reduced seismic capacity (*DS* thresholds) and increased seismic demands, ultimately resulting in an increase in seismic vulnerability level. A similar increase in fragility due to corrosion is also observed for Slight and Extensive *DSs* for the 50-year corroded frame.

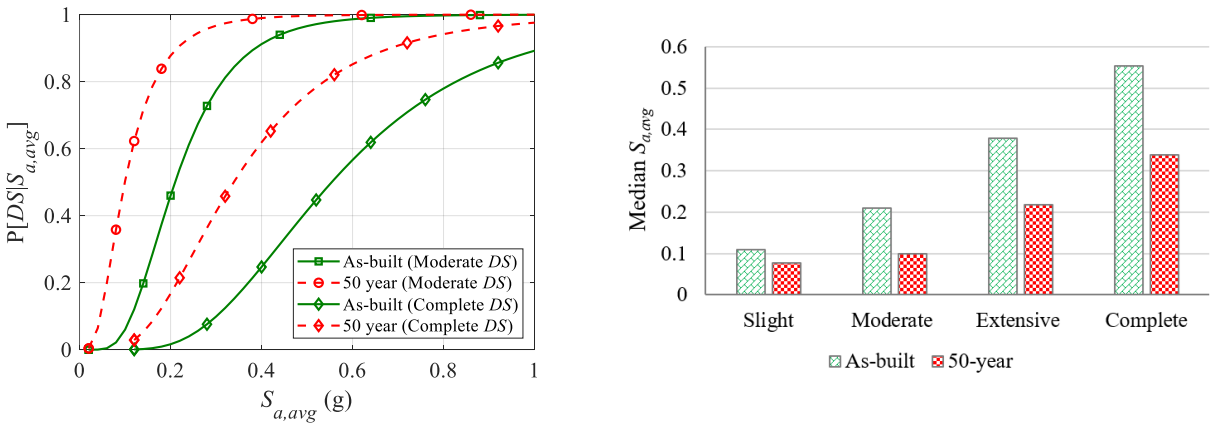

(a) (b)

Figure 6. Comparison of Moderate ad Complete DSs fragility curves for as-built and 50-year frames, and (b) Comparison of median $S_{a,avg}$ of various DSs for as-built and 50-year frames.

Figure 6 (b) shows the median ($S_{a,avg}$ value corresponding to 50% probability of exceeding a specific *DS*) of the fragility curves for the as-built, and 50-year corroded frames. The median $S_{a,avg}$ of 50-year frame are 30%, 53%, 43%, and 38% lower (indicating an increase in vulnerability) than the as-built frame for Slight, Moderate, Extensive, and Complete *DSs,* respectively. Moreover, when compared with the as-built frame, the 50-year frame exhibits greater dispersion [$\zeta(t)$] in their fragility curves due to higher variations in demand [$\beta_D(t)$], capacity [$\beta_C(t)$], and PSDM slope [$b(t)$]. In summary, the findings underscore the considerable impact of corrosion-induced deterioration on the failure mechanisms and seismic vulnerability of low-ductility RC frames, and deterioration aspects must be considered for the lifetime seismic vulnerability assessment of building stocks in earthquake-prone regions.

5 Conclusions

This study assesses the effect of corrosion-induced deterioration on the failure modes and seismic fragility of low-ductility reinforced concrete (RC) frames. Corrosion significantly diminishes the lateral load-carrying capacity of RC components, increasing the chances of non-ductile shear failure of columns. Over 50 years, chloride-induced corrosion results in an average reduction of 19% and 38% in the cross-sectional area of longitudinal and transverse reinforcements, respectively. Moreover, corrosion also leads to secondary effects, such as a 79% reduction in cover concrete strength, a 10% reduction in steel strength, a 67% reduction in ultimate steel strain, and a 25% reduction in shear strength within RC columns. Using a validated numerical model, this research also presented the influence of earthquake records on the various failure scenarios of non-ductile designed deteriorated RC columns within the case-study frame. NLTHA results reveal that corrosion changes the failure mechanism of RC columns from flexure to flexure-shear, and peak drift exhibits a substantial increase (approximately 127%) following 50 years of corrosion exposure when compared to the as-built condition. Non-linear static analyses results reveal that corrosion impairs the lateral load capacity of RC frames, with a 25% mean reduction observed after 50 years of corrosion compared to the as-built condition. Additionally, *DS* thresholds for Slight, Moderate, Extensive, and Complete *DSs* experience a reduction of 19%, 43%, 30%, and 24%, respectively, in the 50-year corroded RC frame. Finally, seismic fragility curves are developed by utilizing the results of probabilistic seismic demand models and *DSs* thresholds. Results reveal a significant increase in the vulnerability of the 50-year frame compared to the as-built frame. The median spectral acceleration of 50-year frame are 30%, 53%, 43%, and 38% lower (indicating an increase in vulnerability) than the as-built frame for various *DSs*. Future work should investigate the non-uniform distribution of corrosion within RC structural element and spatial correlation among building components for lifetime seismic vulnerability assessment of building frames.

6 Acknowledgment

The first author and the third author would like to acknowledge the funding from Science and Engineering Research Board, Department of Science and Technology, India through Grant Nos. SRG/2021/001574 and CRG/2021/000777 respectively for this work.

7 References

ACI-318-89. (1989). *Building code requirements for reinforced concrete and commentary (ACI 318-89/ACI 318R-89)*. American Concrete Institute, Detroit.

Andisheh, K., Scott, A., & Palermo, A. (2016). Seismic behavior of corroded RC bridges: Review and research gaps. *International Journal of Corrosion*, 1–22.

Angst, U. M. (2018). Challenges and opportunities in corrosion of steel in concrete. *Materials and Structures*, *51*, 1–20.

Apostolopoulos, C. A., & Papadakis, V. G. (2008). Consequences of steel corrosion on the ductility properties of reinforcement bar. *Construction and Building Materials*, *22*(12), 2316–2324.

Aycardi, L., Mander, J., & Reinhorn, A. (1994). Seismic resistance of reinforced concrete frame structures designed only for gravity loads: experimental performance of subassemblages. *ACI Structural Journal*, *91*(5), 552–563.

Bracci, J. M., Reinhorn, A. M., & Mander, J. B. (1995). Seismic resistance of reinforced concrete frame structures designed for gravity loads: performance of structural system. *ACI Structural Journal*, *92*(5), 597–609.

Cornell, C., Jalayer, F., Hamburger, R. O., & Foutch, D. A. (2002). Probabilistic basis for 2000 SAC federal emergency management agency steel moment frame guidelines. *Journal of Structural Engineering*,

128(4), 526–533. http://ascelibrary.org/doi/abs/10.1061/(ASCE)0733-9445(2002)128:4(526)

Coronelli, D., & Gambarova, P. (2004). Structural assessment of corroded reinforced concrete beams: modeling guidelines. *Journal of Structural Engineering*, *130*(8), 1214–1224.

Couto, R., Requena-García-Cruz, M. V., Bento, R., & Morales-Esteban, A. (2020). Seismic capacity and vulnerability assessment considering ageing effects: case study—three local Portuguese RC buildings. *Bulletin of Earthquake Engineering*, *19*, 6591–6614.

Davis, C., Keilis-Borok, V., Kossobokov, V., & Soloviev, A. (2012). Advance prediction of the March 11, 2011 Great East Japan Earthquake: A missed opportunity for disaster preparedness. *International Journal of Disaster Risk Reduction*, *1*, 17–32.

Di Sarno, L., & Pugliese, F. (2020a). Numerical evaluation of the seismic performance of existing reinforced concrete buildings with corroded smooth rebars. *Bulletin of Earthquake Engineering*, *18*(9), 4227–4273.

Di Sarno, L., & Pugliese, F. (2020b). Seismic fragility of existing RC buildings with corroded bars under earthquake sequences. *Soil Dynamics and Earthquake Engineering*, *134*, 106169.

Dizaj, E. A., Madandoust, R., & Kashani, M. M. (2018). Probabilistic seismic vulnerability analysis of corroded reinforced concrete frames including spatial variability of pitting corrosion. *Soil Dynamics and Earthquake Engineering*, *114*, 97–112.

Du, Y. G., Clark, L. A., & Chan, A. H. C. (2005). Residual capacity of corroded reinforcing bars. *Magazine of Concrete Research*, *57*(3), 135–147.

Duracrete. (2000). *Probabilistic Performance Based Durability Design of Concrete Structures: Final Technical Report* (Document BE95-1347/R17). The European Union – Brite EuRam III.

Elwood, K. J. (2004). Modelling failures in existing reinforced concrete columns. *Canadian Journal of Civil Engineering*, *31*(5), 846–859.

Freddi, F., Ghosh, J., Kotoky, N., & Raghunandan, M. (2021). Device uncertainty propagation in low-ductility RC frames retrofitted with BRBs for seismic risk mitigation. *Earthquake Engineering & Structural Dynamics*, *50*(9), 2488–2509.

Freddi, F., Tubaldi, E., Ragni, L., & Dall'Asta, A. (2013). Probabilistic performance assessment of low-ductility reinforced concrete frames retrofitted with dissipative braces. *Earthquake Engineering & Structural Dynamics*, *42*(7), 993–1011.

Jeon, J. S., Lowes, L. N., DesRoches, R., & Brilakis, I. (2015). Fragility curves for non-ductile reinforced concrete frames that exhibit different component response mechanisms. *Engineering Structures*, *85*, 127–143.

Koch, G., Varney, J., Thompson, N., Moghissi, O., Gould, M., & Payer, J. (2016). International measures of prevention, application, and economics of corrosion technologies study. *NACE International*, *216*, 2–3.

McKenna, F., Fenves, G., & Scott, M. (2000). Open system for earthquake engineering simulation. In *University of California, Berkeley, CA*.

Pitilakis, K. D., Karapetrou, S. T., & Fotopoulou, S. D. (2014). Consideration of aging and SSI effects on seismic vulnerability assessment of RC buildings. *Bulletin of Earthquake Engineering*, *12*(4), 1755–1776.

Shekhar, S., Freddi, F., Ghosh, J., & Lad, D. (2023). Influence of Corrosion on Failure Modes and Lifetime Seismic Vulnerability Assessment of Low-Ductility RC Frames. *Earthquake Engineering & Structural Dynamics*, 1–23.

Shekhar, S., Ghosh, J., & Ghosh, S. (2020). Impact of design code evolution on the failure mechanism and seismic fragility of highway bridge piers. *Journal of Bridge Engineering, ASCE*, *25*(2), 04019140.

Smerzini, C., Galasso, C., Iervolino, I., & Paolucci, R. (2014). Ground motion record selection based on broadband spectral compatibility. *Earthquake Spectra*, *30*(4), 1427–1448.

Stewart, M. G. (2004). Spatial variability of pitting corrosion and its influence on structural fragility and reliability of RC beams in flexure. *Structural Safety*, *26*(4), 453–470.

Stewart, M. G., & Rosowsky, D. V. (1998). Time-dependent reliability of deteriorating reinforced concrete bridge decks. *Structural Safety*, *20*(1), 91–109.

Thoft-Christensen, P. (2004). Modelling of Corrosion Cracks. *In Information Processing: Recent Mathematical Advances in Optimization and Control: Articles from the IFIP TC 7 Conference on System Modelling and Optimization*, 25–33.

Vu, N. S., & Li, B. (2018). Seismic Performance of Flexural Reinforced Concrete Columns with Corroded Reinforcement. *ACI Structural Journal*, *115*(5), 1253–1266.

Wu, J., Li, N., Xie, W., Zhou, Y., Ji, Z., & Shi, P. (2014). Post-disaster recovery and economic impact of

catastrophes in China. *Earthquake Spectra*, *30*(4), 1825–1846.

Zhang, Y., Ayyub, B. M., & Fung, J. F. (2022). Projections of corrosion and deterioration of infrastructure in United States coasts under a changing climate. *Resilient Cities and Structures*, *1*(1), 98–109.